Response of Boost Converters Under Fission-Spectrum Neutron and Gamma Radiation

Matthew Niichel, *1stLt, United States Space Force, True Miller, Purdue University, Brian Jowers III, Purdue University Robert Cooper, PhD, Naval Surface Warfare Command Crane, and* Stylianos Chatzidakis, *PhD, Purdue University*

Abstract—**Radiation testing of microelectronics remains essential for ensuring reliability in environments such as space and nuclear power systems. One critical component found in many systems is the metal oxide semiconductor field-effect transistor (MOSFET). While work has been conducted on early MOSFET designs, there remains a gap in three key areas: testing modern power MOSFETs, collecting live test data, and evaluating components in combined radiation environments. Using modern components ensures that systems currently in use, both public and private, are better protected against radiation damage. Live monitoring allows observation of single-event effects and transient behavior not detectable through post-irradiation analysis. Additionally, conducting experiments in fission-spectrum neutron and gamma environments better replicates real-world conditions. While the literature addresses each of these topics separately, this work combines them by live-testing a boost converter circuit composed of a MAX1932 gate driver and a BSS119N N-type MOSFET under both neutron and gamma radiation. Testing was performed at the Purdue University Reactor Number One (PUR-1) and the Hopewell Co-60 irradiator, evaluating the circuit's response to gamma total ionizing dose (TID), thermal neutron-induced transients, and environmental temperature. Live monitoring displayed real-time transients, degradation, and recovery behavior. Results indicate gamma radiation plays a dominant role in circuit degradation. However, when considering the dose dependent degradation, the combined radiation environment of PUR-1 induces failure with 34.8% less dose when compared to the Co-60. Suggesting neutron activation is contributing to secondary gamma dose or ^{10}B (n,α) reaction damage. While Co-60 testing remains critical, thermal neutron facilities may offer a useful, cost-effective screening method for identifying gamma-sensitive components.**

Index Terms—**Radiation testing, boost converter, MOSFET degradation, total ionizing dose (TID), neutron activation, thermal neutrons, gamma irradiation, annealing, live monitoring, PUR-1, Co-60 irradiator, microelectronics reliability.**

I. Introduction

Radiation testing of microelectronics is increasingly relevant as modern electronics pervade a number of critical systems that operate in harsh environments. This is in tension with some commonly held misconceptions within the microelectronics industry that components have become less susceptible to radiation over time [1], [2]. This is not an unfounded claim, as many efforts have been taken to mitigate radiation induced upsets in a variety of electrical components through manufacturing processes or conformal coatings [3], [4]. However, much of the work has focused on the component level and has lacked diversity in the radiation environment considered. Furthermore, most publicly available work emphasizes simulation derivations over experimental data. Combined, these topics leave many stones unturned in the realm of microelectronics evaluation under irradiation.

While a radiation-induced failure at the component level cannot be discounted, entire systems have a rich interplay of multiple time-scale effects on the integrated components [5]. As a result, the radiation-induced event may appear significantly different to the end-user than simply an open-circuit or a short-circuit response observed in an individual component. While ultimately the designer cares about the most susceptible element, the end-user cares about how their experience is affected and what performance can be expected out of a device subjected to a radiation environment.

Boost converter circuits are found in a multitude of electronics, from telecommunications to the power grid. While the complexity of the circuits varies among applications, their purpose remains constant. Boost converters act as a means of stepping up direct current voltage for power applications. They act analogously to the alternating current step-up transformer. Due to their widespread use in both space and nuclear power systems, boost converter circuits provide an excellent case study for the propagation of induced effects in a combined neutron and gamma radiation environment [6] [7].

The interest in combined environments stems from realistic operating conditions, such as digital sensors used for instrumentation and control of reactors, space missions, or weapon detonation. The radiation field in real operating environments is rarely a single particle type (nor monoenergetic). Therefore, using both neutrons and gammas for system evaluation moves laboratory testing closer to a scenario in which systems would be subjected to during operation. One of the objective problems with this type of evaluation is attributing the effects to each particle. As a result, efforts are made to recreate the experiment in environments of solely neutrons or gammas. However, neutron interactions with matter produce secondary gammas which are difficult to isolate from the testing system.

II. Background

It has recently been demonstrated by El-Azeem and El-Basit that Co-60 gamma radiation significantly degrades the performance of similar MOSFET-based boost converters [8]. This work implemented a C2M0280120D SiC MOSFET and focused on the switching characteristics of the FET, the change in drain current, and the variation in circuit capacitance as a

function of gamma dose up to 600 kRad(Si). Unfortunately, they did not consider neutron effects. Similar to other literature, the threshold voltage (V_{th}) decreases for an enhancement-type FET device [9]. This results in a MOSFET used as a switch to "turn on" for a lower applied gate voltage (V_g). The drain current is also noted to increase as a function of dose. This signifies the decrease in resistance value across the drain to source (R_{DS}). In the "off" state, a large R_{DS} is desired to maintain the integrity of the switching effect. Finally, the circuit capacitance has been identified as increasing with dose [8] [10]. This value results in a reduced ripple voltage across the boost converter output. While the other two effects are typically regarded as negative, the reduced ripple can be useful for applications where the output voltage needs to be steady. It is important to note that El-Azeem and El-Basit did not consider live radiation monitoring. Rather, circuits were subjected to various doses and then measured post-exposure [8].

In 2002, Adell *et al.* classified the effects of total ionizing dose on power MOSFETs [11]. They recognized that significant work had been conducted on classical MOSFETs, but at the time, more work was required to understand power MOSFETs. They considered both boost and buck converter operation post-exposure to a dose of 100 kRad (Si) of X-rays. They reported that the mode of operation of the converter circuit affected the rate of degradation of circuit performance. Where boost converters drastically underperformed buck converters when compared to no dose. This was supported by the change in the circuit output voltage (V_{out}) and V_{th}. They also identified that the most limiting component for single-event transients in the circuit was the pulse width modulating (PMW) V_g driver. Simulations and experimental results described the V_{out} of both circuit types decreasing with more noise induced into the PMW driver.

In 2017, Lv *et al.* considered the effect of both fast and thermal neutrons on the optical changes in the material and electrical defects in gallium-nitride-type (GaN) PIN diode commonly found in radiation detectors [12]. While not a MOSFET, PIN diodes are increasing in popularity as power rectifying semiconductors. They noted that while both thermal and fast neutrons induce damaging effects, thermal neutrons disrupted the device more electrically and fast neutrons materially when compared to unirradiated devices.

In 2023, Metiva *et al.* studied the failure of the total Starlink satellite constellation in low-Earth orbit due to ionizing radiation from coronal mass ejections and naturally occurring space radiation [13]. Though they did not consider MOSFET failure, it is related to the failure of off-the-shelf components in a radiation environment. They claim that while some of the units failed due to upper-atmospheric drag, they found a strong correlation between space weather events and Starlink failures. They did not contain the mechanism of failure, but alluded to the current relevance of designing systems for radiation environments.

A foundational finding from previous literature states that many off-the-shelf components can receive 15 kRad of gamma TID before failure. There is little publicly available information on neutron data for similar components. It was proposed that the combined radiation environment would induce synergistic effects on the device under test (DUT). [17]

While there are relevant studies considering the single event effects of radiation, one aspect that must not be downplayed is the availability of the facilities to conduct these experiments. Unclassified studies prepared by NASA and the Strategic Radiation Hardened Electronics Council both call to action the United States Federal Government to invest in radiation testing facilities to relieve the current over-subscription, and a full backup of the domestic radiation testing timeline. Without significant capital in fiscal year 2019, the demand would outpace the capacity by 2023. [7] [8]

In summary, extensive work has been conducted to classify the radiation-induced effects on MOSFETs; however, the studies discussed may be missing the full spectrum of effects by not conducting live monitoring or considering combined radiation environments. [24] This article aims to explore the use of live monitoring and combined radiation environments to better understand how circuits fail in real-time and in an environment that more closely resembles operational conditions.

III. Experimental Setup

The following evaluations focus on the Maxim MAX1932 driver and a converter circuit using the commercially available BSS119N N-type silicon MOSFET. These evaluations include monitoring the output voltage of the boost converter circuit as a function of radiation exposure and temperature. Additionally, the measurement of the resistance across the MOSFET and the feedback resistor as a function of exposure and temperature. The full component-level diagram for the boost converter circuit is shown below in Fig. 1.

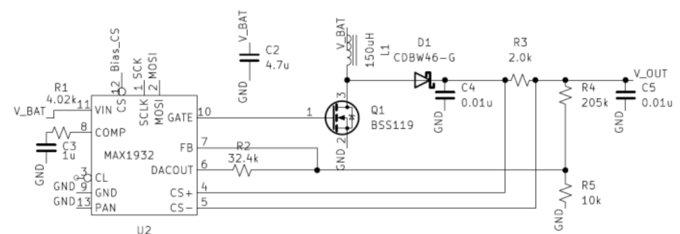

Fig. 1 Component level schematic of MAX1932 and BSS119N MOSFET boost converter circuit [25].

There are numerous challenges associated with conducting radiation tests in general. However, another set of obstacles are presented while attempting to collect live results while under irradiation. One issue is protecting the recording instruments from the effects of ionizing radiation. The measurement methods for this device are derived from the IEEE standard 802.3af (Power over Ethernet) and are monitored using Arduino hardware and MATLAB-based software [25].

There are several benefits to conducting live tests as opposed to taking measurements post-irradiation and comparing them to the controlled measurements. The most obvious benefit is the ability to more accurately monitor single-event transients in the system as they occur. This can be used to better understand how the device operates in a realistic environment [26]. Many devices may also exhibit annealing, or "self-healing," following the removal from the radiation environment. If this occurs, some induced effects may not be observed [27].

A less obvious advantage of live monitoring lies in the increased cost associated with static testing. Unlike live testing, static methods require multiple separate irradiation trials. Devices are exposed to a target dose, removed from the beam, and then measured. This process is repeated across a range of dose levels to establish a meaningful trend. The repetition significantly increases the time required to complete a full test campaign, which directly raises the overall cost. The perception that developing the equipment to conduct live tests increases the test budget may hold for individual electronic components. However, for large systems, the cost savings for utilizing fewer DUTs may outweigh any cost associated with live-monitoring.

IV. Radiation Environments

A. Selection Criteria

The selection of the radiation environments to conduct tests had three criteria. Foremost, availability was of chief concern. As discussed, finding radiation facilities that can perform experiments is increasingly difficult due to oversubscription and the classified nature of some sources. The second selection criterion was how well each source was characterized for the radiation environment. A test is only successful if the dose and type of particle are known. Finally, the source strength of the environment was used to rule out certain facilities. If it would take an unreasonable amount of time to conduct a test to MIL-STD-750D, the source was excluded [28]. As a result, three facilities were selected. The Purdue subcritical pile, the Purdue research reactor, and the NSWC Crane Co-60 irradiator.

B. Purdue Subcritical Pile

The Purdue subcritical pile was rearranged in late 2024 to accommodate a testbed for microelectronics testing with thermal neutron flux. The radiation environment of the pile was characterized by using a series of gold and indium foils for neutron measurements. A Geiger-Muller detector and a sodium-iodide scintillating detector were used for gamma measurements. It was determined that the maximum neutron flux achievable within the testbed was 1.2×10^4 cm^{-2}×s^{-1}. The gamma energy spectrum was consistent with uranium-235 fission with an exposure of 28 mR/hr. [29] Five tests were conducted over a two-week period with no deviation in performance compared to the controlled measurements. While this environment may have some utility in testing memory upsets, it was ultimately deemed not appropriate for further analysis of the boost converter circuit performance.

C. Purdue Reactor Number One (PUR-1)

The 10-kW research reactor hosted at Purdue University contains a 7.6 cm diameter PVC drop tube that allows for limited irradiation tests. The position of the drop tube allows a test sample to be placed at the midline and a straight-line distance of 30.0 cm from the core.

Gold foil and cadmium cover tests were conducted following ASTM standard E262-17 to determine the thermal and epithermal neutron flux in the drop tube for the reactor at 60% power [30]. The thermal neutron flux was found to be 2.78×10^7 cm^{-2}×s^{-1}and the epithermal neutron flux 2.49×10^5 cm^{-2}×s^{-1}s [30].

It should be noted that it is typical to report neutron fluence as 1-MeV equivalent (Si) for radiation hardness testing. This process is outlined in ASTM E277-09, and the relationship is

$$\Phi_{eq,silicon} = \frac{\int_0^\infty \Phi(E)\, F_{D,silicon}(E) dE}{F_{D,Eref,silicon}} \quad (1)$$

where, $\Phi(E)$ is the incident neutron fluence spectrum, $F_{D,Silicon}(E)$ is the energy-dependent displacement damage in silicon, and $F_{D,Eref,Silicon}$ is the neutron displacement reference value (95 MeV × mbarn for silicon) [31]. The neutron fluence spectrum within the core was calculated using MCNP6.3 to produce the neutron lethargy as a function of energy [32]. However, it is important to note that MCNP outputs neutron tallies as *neutrons per source particle.* **Error! Reference source not found.** displays the neutron lethargy found at the center of PUR-1, and **Error! Reference source not found.** displays the silicon microscopic displacement Kerma factor as a function of energy. Using equation (1), the 1 MeV equivalent fluence in PUR-1 is 8.32×10^{-5} cm^{-2} per source particle. The value can be used to estimate the Flux at the drop tube location using

$$\phi_{tube} = \frac{\Phi_{eq,silicon} P\nu}{E_f 4\pi r^2} \quad (2)$$

where, ϕ_{tube} is simulated neutron flux at the test location, P is the reactor power in watts, ν is the neutron reproduction factor (2.43 for uranium-235), E_f energy per fission in joules, and r is the radius from the reactor. Using equation (2), the 1 MeV equivalent flux at the test location is estimated to be 3.35×10^6 cm^{-2}×s^{-1}. The result lies within the range of experimental measurements, but likely overestimates the neutron flux, as the MCNP calculation was performed within the reactor core and does not account for moderation in the coolant. In this context, the MCNP data serves as a first-order approximation for comparison with gold foil activation measurements.

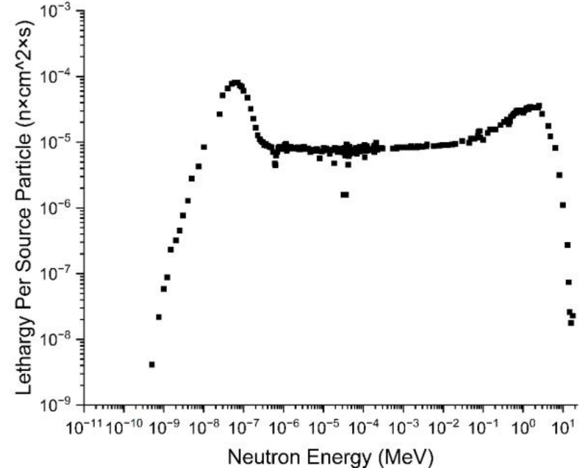

Fig. 2 MCNP PUR-1 neutron lethargy per energy. Note, lethargy allows neutron data to span multiple energy decades uniformly, minimizing thermal bias.

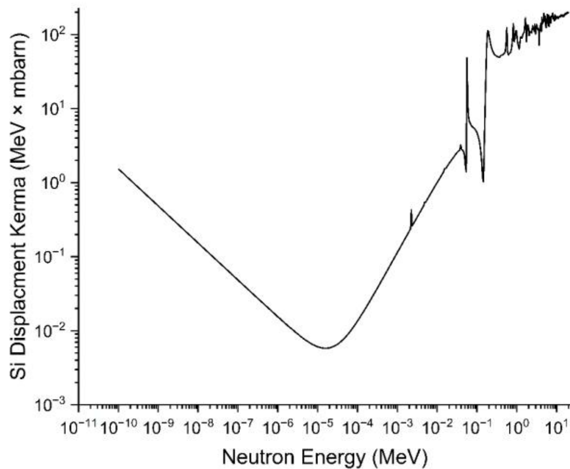

Fig. 3 Silicon microscopic displacement Kerma factor used to determine equivalent fluence.

Multiple $^6LiF_2$ and $^7LiF_2$ thermoluminescent dosimeters were placed in the drop tube at 1% power for 1 minute. It is essential to note that these dosimeters are designed to report in Rem as radiation worker dosimetry. Subsequently, the total gamma dose measurement is estimated to be 14.29 Rad (quality factor of 1), and the neutron dose is 1.32 Rad (quality factor of 10). Linear extrapolation for time is then used, given a constant reactor power of 59.94% ± 0.84% measured through the PUR-1 instrumentation. This interpolation can be used to determine the total ionizing dose or the total thermal neutron fluence for any test irradiation time. On average, it was determined that for a 60-minute run at 60% PUR-1 power, the TID is 51.47 kRad and the neutron dose is 4.68 kRad.

D. *Hopewell Cobalt-60 Irradiator*

The Hopewell irradiator contains a central well with a concentric ring of Co-60, which is used to expose gamma rays to a device under test. Besides the physical construction and ability to shield the technician, there is little variation from other gamma irradiators. The energy of the isotope is a critical aspect of any TID experiment because the effects of radiation are proportional to the energy deposited. MIL-STD-750D specifically calls for radiation testing to use cobalt-60 due to the large gamma photopeaks of 1.17 MeV and 1.33 MeV.

The military standard also describes the ionizing dose in silicon to exist between 50 and 2000 Rad/s (Si). Like the 1MeV equivalent neutron fluence, the TID range is based upon a strategic radiation spectrum. The Hopewell irradiator provides a dose in silicon that adheres to MIL-STD-750D. The TID chamber has a thermocouple that can determine the rise in environmental temperature from photo interactions. While the reactor does not have this feature, the pool of water and a reduced gamma dose do not appreciably raise the environmental temperature, unlike the TID chamber.

V. Control And Thermal Effects

The ultimate goal of the boost converter is to increase the V_{out} from 5 V_{DC} to 34.8 ± 1.2 V_{DC}. While the MAX1932 and BSS119N MOSFET are capable of providing up to 100 V_{DC}, the particular configuration was selected to power a silicon photomultiplier rated for 35 V_{DC} [33], [34]. Collecting the controlled circuit response and the response to an elevated environmental temperature was of chief concern for evaluating degradation due to radiation effects. Several control measurements at room temperature were taken across the V_{out} for the boost converter to establish both the stability and average value. The values were digitally recorded, which provides measurements at discrete values. The result for the control test boards is displayed in Fig. 4.

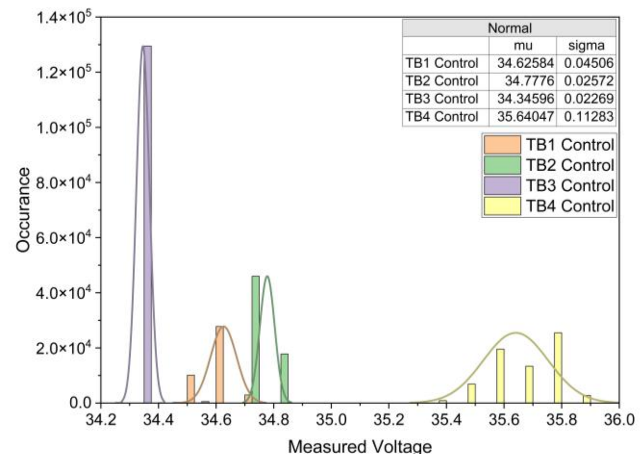

Fig. 4 Distribution of pre-irradiation control measurements of Vout for the four test boards at 25°C. The sampling period is 3.4 seconds per measurement. The data for each control were fit to a normal distribution, and the fit parameters are provided in the table.

It was determined that the unbiased R_{DS} and R_{SD} were 1.72 MΩ and 4.43 MΩ, respectively at 25 °C. The datasheets for the MAXIM and FET devices describe a strong temperature dependence. The MAX1932 specifically recommends negative temperature compensation parallel to R_5 for feedback amplified by an op-amp [33]. An experimental temperature-controlled environment was established using a hot plate and a sheet of copper to transfer heat effectively to the boost converter circuit. The surface temperature of the FET casing was measured with a period of 30 seconds. Additionally, the unbiased resistance of the R_5 and R_{DS} were taken at the same interval. While most of the resistors in the system were identified to have temperature dependence, the two identified components were deemed most likely to propagate the temperature-induced effects. The record of R_5 and R_{DS} as a function of FET surface temperature are plotted in Fig. 5 and Fig. 6, respectively.

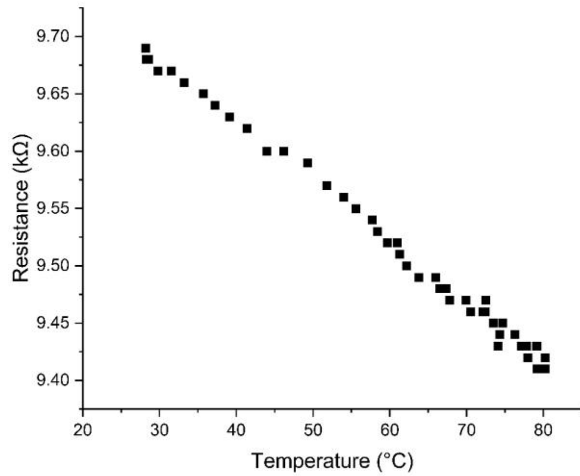

Fig. 5 Unbiased MOSFET R5 Resistance During 80 °C. Note that the ordinate has been zero suppressed.

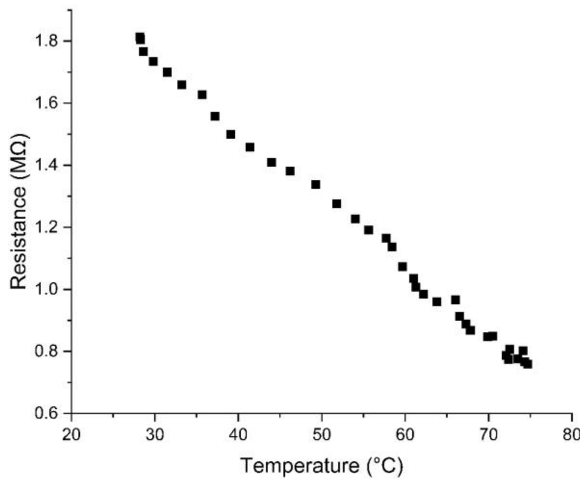

Fig. 6 Unbiased MOSFET Drain-to-Source Resistance During Heating to 80 °C. Note that the ordinate has been zero suppressed.

To prevent damage to the measurement device, resistance was not measured while the boost converter was under power. However, the V_{out} was measured for a heat-up period and a subsequent cool-down period. The optically measured surface temperature of the FET device is plotted in Fig. 7, with the curve fit of heating and cooling provided in Table I and the following equations (2) for heating and (3) for cooling. The measured V_{out} in **Error! Reference source not found.** as a temporal function of temperature and Table II for curve fitting.

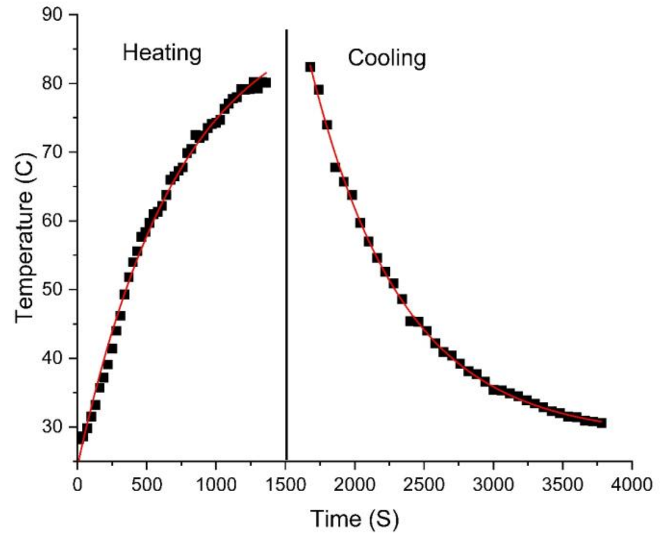

Fig. 7 Surface temperature of the MOSFET device during the heating to 80 °C and cooling to 28 °C cycle.

$$Y = A + B\,(1 - e^{-Cx}) \quad (2)$$
$$Y = A + B(e^{-Cx}) \quad (3)$$

Table I
Summary of Temperature Cycle Curve Fitting

Descriptor	Heating	Descriptor	Cooling
R^2	0.993	R^2	0.998
A	24.25± 0.64	A	28.51±0.30
B	67.96± 1.39	B	688.80±31.85
C	735.34±38.74	C	660.30±12.07

We fit the surface temperature data of the FET to an exponential form of Newton's heating and cooling law as,

$$T(t) = T_\infty + \Delta T\left(1 - e^{-\frac{t}{\tau}}\right) \quad (4)$$
$$T(t) = T_\infty + \Delta T\left(e^{-\frac{t}{\tau}}\right) \quad (5)$$

where T_∞ is the ambient temperature, ΔT is the difference between the hot plate and ambient temperature, τ is the material and geometric constant, and t is the time.

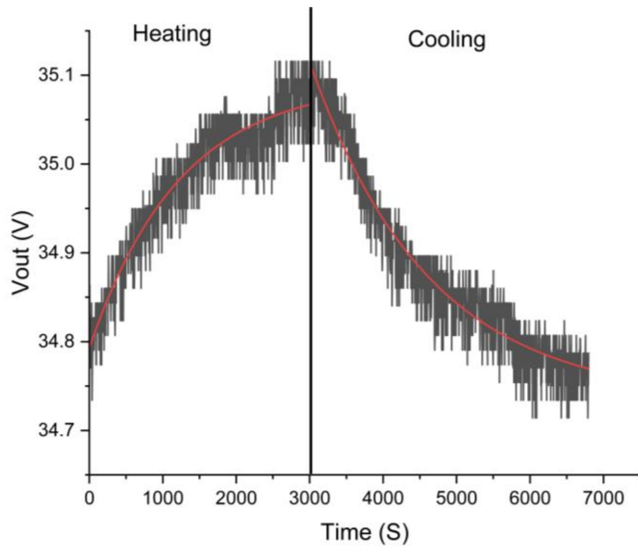

Fig. 8 Measured Vout during heating and cooling cycle. Note that the ordinate is zero suppressed.

Table III
Summary of Temperature Cycle Curve Fitting

Descriptor	Heating	Descriptor	Cooling
R^2	0.873	R^2	0.922
A	34.79± 0.01	A	34.73±0.01
B	0.30± 0.01	B	2.47±0.14
C	1227.19±57.00	C	1681.82±51.32

The measured V_{out} strongly correlates with the measured surface temperature of the FET device. However, there appears to be a 1500-second time delay for heating and a 3000-second delay for cooling between the surface temperature and the change in V_{out}. It is speculated that the SiO_2 and plastic casing of the FET device act as an insulator and transmit the heating signal more slowly relative to the measured surface temperature. Table III provides a summary of the curve fit temperature coefficient (κ) for the heating cycle, by taking the inverse of the values labeled “C” in Tables I and II. Where the change in voltage is assumed to be due to the internal temperature change.

Table IIIII
Summary of Temperature Coefficients

Descriptor	Temperature Coefficient (s^{-1})
Surface – Heating	$1.36x10^{-3}$
Surface – Cooling	$1.51x10^{-3}$
Internal – Heating	$8.15x10^{-4}$
Internal – Cooling	$6.24x10^{-4}$

The reported change in resistance across R_5 and R_{DS} is the proposed cause of the shift in voltage for increased environmental temperature. R_5, in particular, may be the most contributing component to this variation in operation. This is due to the component’s relationship with the MAX1932 feedback comparator input.

It is proposed that the inclusion of a 10 kΩ positive temperature coefficient thermistor as a substitution for R_5 will aid in mitigating any significant contribution to the variation of V_{out} because of environmental temperature. However, two details should be noted for testing. The circuit output, while temperature dependent, does not have a permanent effect on V_{out} upon returning to ambient conditions. More importantly, the testing environment in PUR-1 does not exceed 30°C, and the TID testing of the Hopewell irradiator does not exceed 47°C for the boost converter test. These combined factors provide evidence that there is a distinct difference between thermal and radiation-induced effects. So long as the change in V_{out} as a result of radiation-induced transients exceeds 1 Volt when compared to the nominal reading of the DUT, then it can reasonably be stated that the effects are due to radiation and not temperature.

VI. Radiation Testing

A. Combined Neutron and Gamma Environment

The objective of radiation testing was to conduct live monitoring for three hours within the PUR-1 reactor or until the DUT was no longer able to provide measurements. PUR-1 was brought up to 60% power (6 kW) before placing the DUT into the drop tube, then lowered to the testing location. This practice ensures that the gamma dose and neutron fluence can be reasonably predicted using a linear relationship with time. While placing the DUT into position and ramping power, the dose and fluence would be non-linear, and the final predicted value would have more uncertainty.

A series of 7 test boards were placed into PUR-1, surviving for an average of 60 minutes with a maximum time of 72 minutes and a minimum of 43 minutes. Test boards 6 and 7 evaluated the power cycling of the boost converter. As a result, their time until failure is not included in the average. However, the output voltage at the time of failure was similar to the first 5 boards. The DUT was considered to have failed when either remote serial communication was lost or when the V_{out} of the boost converter returned to 5 V. Here, 5 V is the same value produced when the MOSFET is in the “off-position” for a long time and the energy in L_1 has been fully discharged.

The measured voltage for test board 2 as a function of neutron fluence is shown in Fig. 9. The general trend of V_{out} was a linear departure from the nominal 34.5 V to 42 V, beginning near 30 minutes. Three independent channels are used to collect data for coincidence; the mean of the signals is displayed as the average. Note that the discontinuities in the voltage signify a soft reset of the DUT lasting less than 30 seconds each. Departure from one standard deviation of the nominal voltage relative to the individual board’s control measurements occurred for a neutron fluence near 1.00×10^{10} cm^{-2}. Table IV provides a summary of the test boards and their failure time.

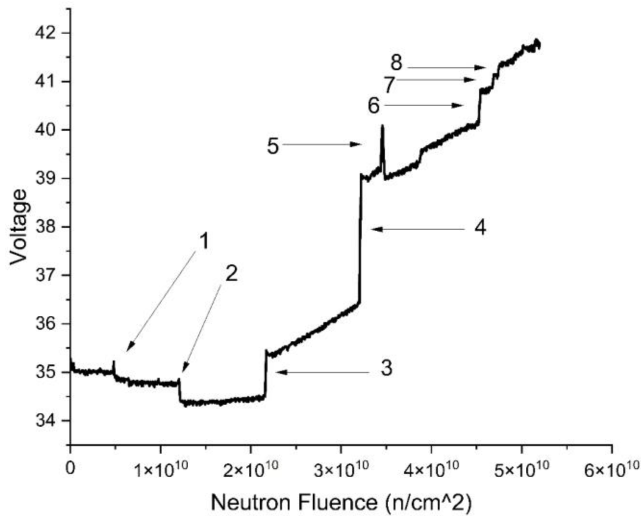

Fig. 9 The mean average of test board 2 V_{out} while subjected to 60% reactor power in PUR-1. Three independent measurements of the voltage were used to generate the mean. Soft resets are numerically labeled. Note that the ordinate and abscissa are zero suppressed.

Table IVV
Summary of Test Board Failures

Test Board Number	Fluence Failure (cm^{-2})	V_{out} Max (V)	Soft Resets
1	7.24×10^{10}	39.4	1
2	1.21×10^{11}	41.7	8
3	8.01×10^{10}	35.2	2
4	1.15×10^{11}	40.6	4
5	1.16×10^{11}	38.8	3
Average	$\mathbf{1.01\times10^{11}}$	**39.2**	**4**
*6	1.35×10^{11}	36.1	1
*7	1.99×10^{11}	40.0	1

Note: Test boards 6 and 7 were used to evaluate boost converter power cycling. Their longevity may not be representative of the remaining boards and has been excluded from the average results.

It was found following test board 3, that a hard reset of the DUT would reestablish serial communication. As a result, post-irradiation measurements were conducted and are displayed in Fig. 10 as a function of time for test board 4. The reduction of the voltage over post-irradiation time occurred in all the boards analyzed following their removal from PUR-1, which suggests some annealing. It is important to note that the follow-on measurements were conducted immediately after PUR-1 was scrammed, preventing any unobserved annealing.

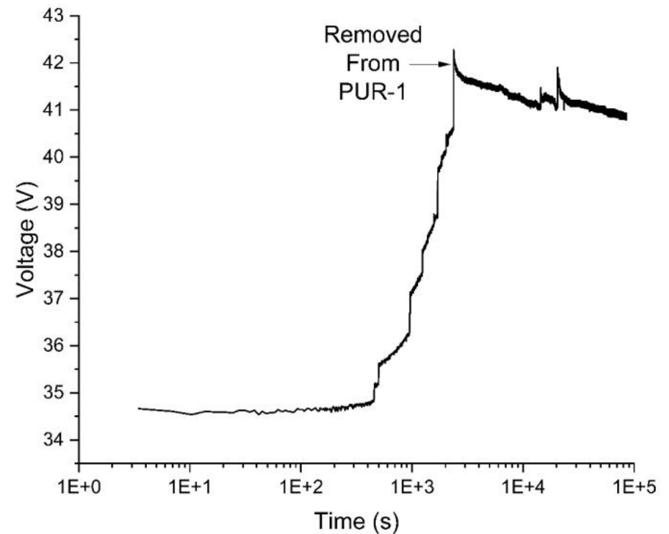

Fig. 10 Test board 4 averaged Vout during and following the removal from PUR-1 at 60% power. Note that the abscissa is now logarithmic and the ordinate is zero suppressed.

When annealing was observed, it was suggested that there may be a temporal and temperature dependence on self-healing. This has been explored in other literature, but remains different for each component [35]. As a result, it was of interest to test if applied heat would further anneal a test board following an initial annealing period at ambient temperature. The same setup discussed previously was used to create an 80°C environment for annealing observation. Fig. 11 shows a similar heating and cooling curve where the baseline V_{out} is the room temperature annealing value. Though more work is warranted in this area of research, it does not appear that providing a heated environment for an intermediate period appreciably anneals the boost converter system beyond the initial ambient period.

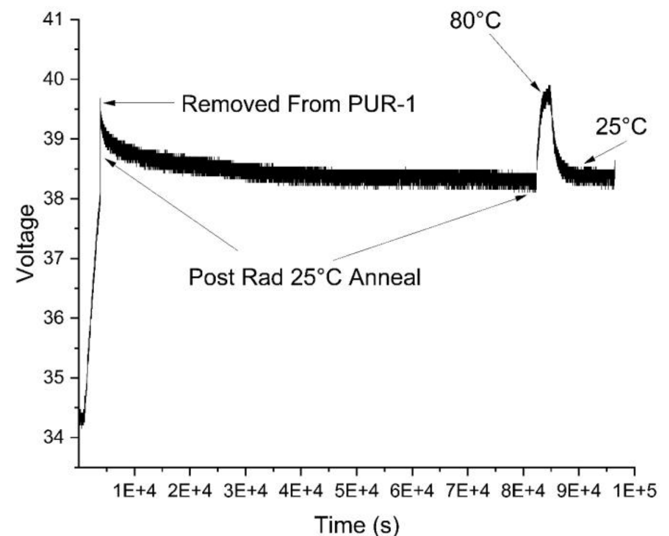

Fig. 11 Test board 8 averaged Vout exploring temperature assisted annealing for an 80 °C environment cycle. The temperature was held for 30 minutes. Note that the ordinate is zero suppressed.

It was also of interest to determine if the effects from PUR-1 could be shifted by filtering out the thermal neutrons using cadmium shielding. The Cd-113 average thermal absorption microscopic cross-section for thermal neutrons is two orders of magnitude larger than the materials that exist in the drop tube. As a result, a 1 mm-thick sheet of cadmium can absorb up to 99.9% of thermal neutrons under 0.55 eV [30]. The remainder of the spectrum that penetrates the shield remains in the epithermal and fast spectrum. However, it should be noted that the capture of the thermal neutrons results in an increased gamma dose from a photopeak at 558 keV [36].

A 0.3 cm-thick cadmium sheet was applied to the drop tube in PUR-1 to effectively remove all of the thermal spectrum in the testing region. Gold foil measurements were once again used to determine the neutron flux. Where foils were placed external and internal to the cadmium shield to measure total and epithermal/fast flux. The respective values for neutron flux at 60% power are 2.63×10^{7} $cm^{-2}\times s^{-1}$ (0.27% uncertainty) and 7.48×10^{5} $cm^{-2}\times s^{-1}$ (0.54% uncertainty). Furthermore, a secondary TLD was placed under the same condition, which reported the gamma dose and neutron dose of 15.03 Rad and 1.32 Rad, respectively. For a 60-minute run at 60% power, the approximate TID is 54.11 kRad, and the neutron dose is 4.75 kRad.

A boost converter circuit was placed in PUR-1 for 68 minutes, and the V_{out} was recorded (Cd PUR-1). These results are presented and compared to test board 4 (PUR-1) and the Co-60 test board in Fig. 12 as a function of dose. The dose rate for both instances within PUR-1 are derived from the TLD measurement by combining the neutron and gamma dose values.

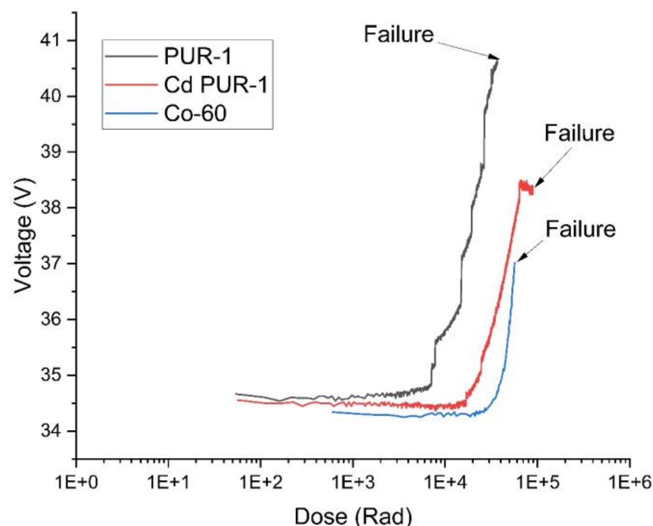

Fig. 12 Vout for each radiation environment as a function of gamma dose and estimated gamma and neutron dose for the reactor. Note that the abscissa is now logarithmic and the ordinate is zero suppressed.

B. Gamma Environment

The objective of Co-60 TID testing was to assist in isolating the particle responsible for the observed transient in the boost converter circuit. The Hopewell source could observe similar effects as PUR-1 but at a significantly accelerated timeframe when compared to the much longer one-hour runs at PUR-1.

Three test boards were subjected to the Co-60 source, and the average test time to failure was 10 minutes. In accord with PUR-1 reactor tests, the reported V_{out} displayed an exponential increase to 37.0 +0.1/-1.2 V and then failed to the default 5 V output, indicating a circuit failure. Due to the total failure of the circuit, a post-irradiation assessment considering annealing could not be performed on these test boards. However, it was found that the value of R_5 remained near the nominal non-irradiated 9.80 kΩ value, but the R_{DS} read as 0 Ω, indicating a MOSFET burnout. The average V_{out} measurements of the 3 for each of the Co-60 tests are shown in Fig. 13.

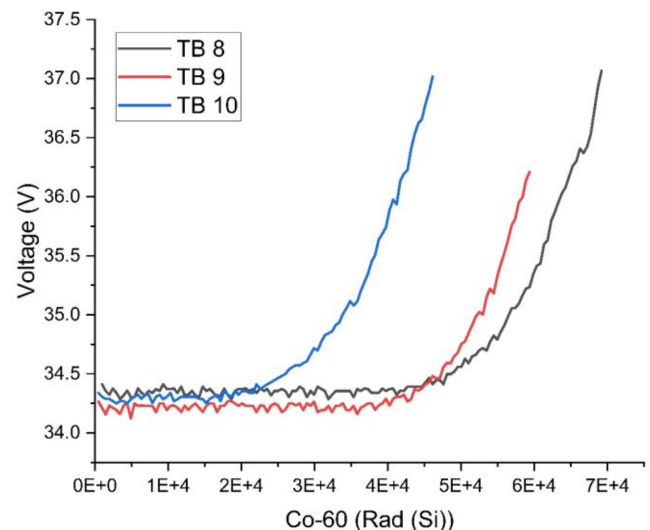

Fig. 13 Recorded V_{out} of boost converters for MIL-STD-750D compliant Co-60 dose rate TID. Note that the y-axis (ordinate) is zero suppressed.

VII. Discussion

Upon conducting the TID experiment, evidence supports that the TID has a significantly larger effect on the boost converter output voltage when considering both time in the environment and the destruction of the DUT during irradiation. This was supported by the accelerated time until failure and inability to conduct post-irradiation measurements. The similar behavior of the output voltage over time and subsequent dose suggests that the induced transient in V_{out} is more affected by gamma radiation than neutrons. However, when the comparison is made as a function of dose, evidence suggests that the combined radiation environment causes premature failure by 34.8% and early onset damage when compared to the failure dose of the most conservative failure among the Co-60 tests.

For the experimental setup in the drop tube, there is little room to add additional shielding. However, given the thermal shielding effects of cadmium, it can be assumed that at 1 mm thickness, the majority of the flux that the shielded test received was greater than 0.55 eV [30]. As a result, the probability of material activation decreases by multiple orders of magnitude for most stable isotopes present, except for the resonance region [37]. We propose that the increased survivability of the shielded

experiment is due to reduced neutron activation and subsequent secondary neutron reactions such as (n,γ), (n,p), or (n,α). These results suggest that thermal neutron effects cannot be dismissed. If TID is the source of the effects observed, then it can reasonably be expected that in a thermal flux, the material activation of the DUT may contribute to the ionizing dose. As a result, it is believed that there are synergistic effects from the combined radiation environment that contribute to deposited energy.

Additionally, there is a time dependence of the activation and the production of decay gammas. The placement of the TLDs in the testing location at the start of PUR-1 operation time most likely did not experience any of the additional dose from these activation products. As 60 seconds was not long enough for the medium and long-lived isotopes to be generated. The problem associated with the use of TLDs for this measurement is the device's dose saturation point. A few minutes in PUR-1 at 1% power would cause a saturation of the device, without taking into account activation.

One solution is to find a dose measurement device that has a saturation point at multiple kRad. However, an alternative solution may be conducting a similar experiment at the end of the one-hour PUR-1 experiment for 60 seconds, as opposed to the beginning. The difference in the recorded dose may provide insight into the contribution from activated materials.

Moreover, due to the proximity of activated components, small activities may have a non-negligible effect on the total dose experienced by the DUT. As a result, it was of interest to future efforts to gather an HPGe gamma spectrum of the DUT immediately following the removal from the neutron flux. Fig. 14 provides the gamma spectrum of the activated board containing the boost converter and accompanying circuits, with the strongest peaks labeled.

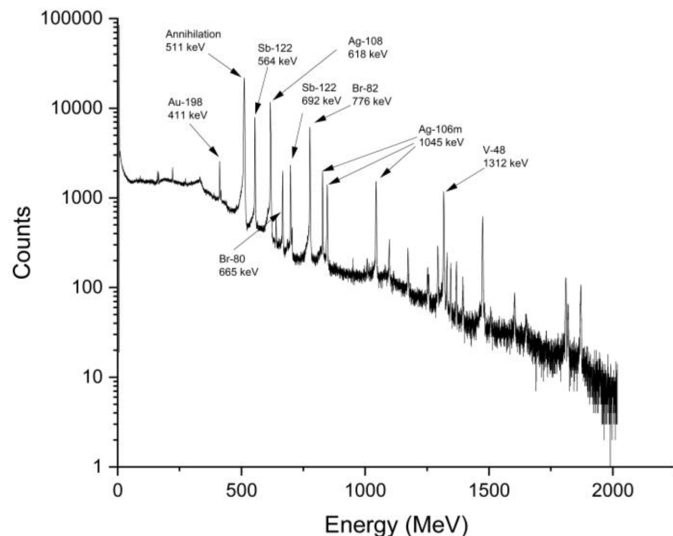

Fig 14. HPGe gamma energy spectrum collected for 600 seconds following a 60-minute exposure in PUR-1. Note that the abscissa is logarithmic.

While the gamma spectrum displayed above does not show many photopeaks above 750 keV, a significant photopeak is present at 511 keV. This signifies the occurrence of pair annihilation, which has the potential to induce damage internally within the DUT. This measurement supports that self-irradiation following neutron exposure may not be negligible. While a fast spectrum will induce activation, the probability is lower than in a thermal spectrum. As a result, this must be a consideration for this and other experiments.

The PUR-1 portion of this test does not exclusively rule out effects from displacement damage, nor the effects from thermal neutrons. However, the results in the TID section strongly correlate with the results from PUR-1. This suggests that the effects that are observed under the reactor conditions are from the gammas, rather than the neutrons. It is therefore suggested that a test in a fast neutron spectrum would provide data that could be used in isolating any effects induced by displacement damage.

It was of interest to compile a preliminary list of metals for MCNP modeling. A Hitachi EA1400 X-ray fluoroscopy (XRF) machine was used to generate the relative weights on an elemental basis. Fig. 15 displays the MOSFET as observed through the XRF machine, and Table V provides the suggested elements by relative weight and their associated 2200 m/s thermal neutron cross-sections, as determined by Brookhaven National Laboratory in 1992 [38]. It should be noted that the X-ray tube internal to the XRF equipment is made of rhodium. It does not have a self-discriminator, so any rhodium found in the spectrum may be discarded. Additionally, the XRF has a low Z-limitation, where materials with Z values less than 11 are not detectable [39]. Boron, which is commonly used as a doping agent for MOSFETs has a large affinity for thermal neutrons (3837 b) and is not detectable by XRF. This analysis did not consider the effects of the (n,α) reaction of boron-10.

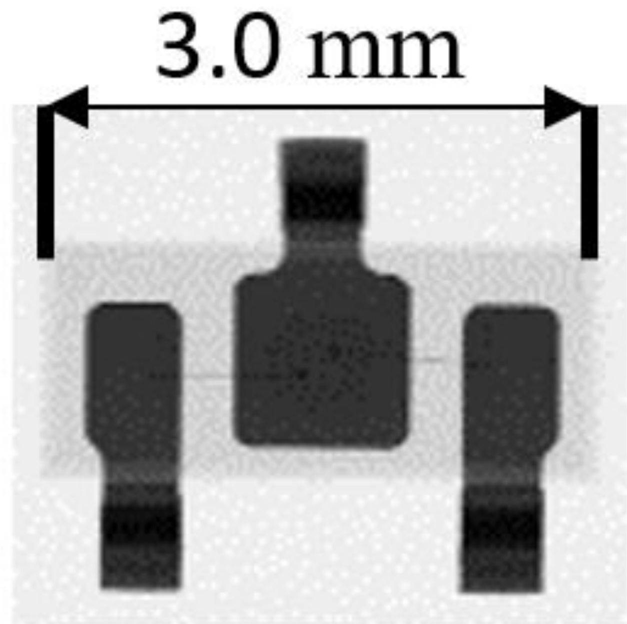

Fig 15. BSS119n MOSFET image generated while under X-ray fluoroscopy.

Table V
XRF Elemental Composition of MOSFET

Element Symbol	Relative Weight (%)	3σ (%)	XS (b)
Si	37.6834	47.138	0.171
Cu	23.4044	17.7039	3.78
Rh	15.9979	12.1015	144.8
Ag	12.9569	9.8011	63.3
Sn	5.0039	3.7859	0.626
Ba	1.8555	1.4247	1.1
Fe	1.0164	0.7693	2.56
V	0.5425	0.4174	5.08
Cr	0.4799	0.366	3.05
Au	0.3307	0.2511	98.65
Sb	0.3023	0.2444	4.91
Zn	0.1972	0.1494	1.11
Ta	0.1688	0.1299	20.6
Ni	0.0489	0.0387	4.49
Br	0.0113	0.0166	6.9

While the results for the cadmium shielded board are not robust at this point, they offer a unique insight into the effects of thermal neutrons on the system. Unlike any of the other boards, there was a period of irradiation during which the results were stable. Due to the gammas from the thermal neutron capture on the cadmium shield, the gamma dose within the shield is 4.87% larger than the bare drop tube. If the transient in V_{out} is solely due to the TID effects, it is hypothesized that the slight uptick in gamma dose from the cadmium shielding should yield similar results or an increased rate in boost converter degradation. However, it is observed that the rate of V_{out} increase is lower, settling at a maximum value of 38.5 V, then settling in a region of stability.

This deviation in the transient behavior of the cadmium shielded board when compared to the unshielded board indicates that there may be a dependence on the thermal neutrons. The mechanism that is likely to be the culprit is the activation of the materials internal to the test board, then subsequent internal gamma exposure as the materials decay. This may be directly the cause of the lower V_{out} value observed. Additionally, due to less TID damage occurring during irradiation, there would be less damage to anneal following time in the reactor. More work is required in this area, but it offers some insight into how thermal neutrons affect microelectronics under combined thermal and gamma sources.

While these results are not definitive enough to disregard MIL-STD-750D tests for fast neutrons or total ionizing dose (TID), there is evidence that thermal sources can cause damage through TID via activation. Due to the limited availability of fast-burst reactors and domestically produced Co-60, along with the high cost of testing, it may not always be practical for microelectronics designers and manufacturers to perform these evaluations. This work contends that more available thermal reactors may be used as a primary means of identifying radiation-soft components. A fabricator may then apply current radiation hardening techniques prior to irradiation time in the military standard sources. This effort would save both development time and money for medium- and low-priority systems, which require a radiation-hardened classification. It may also be worthwhile to develop a secondary classification of components that pass thermal and TID testing, but have not been tested for fast neutrons. A lower grade classification would allow for accelerated fielding of components that need to be deployed immediately or for intermediate-length missions.

The work conducted with the cadmium shielding identified the need for future efforts considering various metal shields. At this point, it is hypothesized that a combination or alloy of metals with high affinity for thermal neutron capture and subsequent high-energy gamma energy may allow for full capitalization of a thermal source, shifting the effects closer to that of Co-60. Perhaps the neutron flux may not be large enough to provide any evidence of transient behavior. However, the neutrons may be used to maximize the high-energy TID to a test article. While the activity alone may not be large enough to act as an independent source of gammas, a casing around a DUT may provide the proximity necessary to induce TID effects. Efforts are currently underway exploring the use of Nickel, Cadmium, and Gadolinium test casings for their large neutron absorption cross-sections and high-energy gamma production.

VIII. Conclusion

This study has demonstrated that the combined radiation environment of thermal neutrons and gamma rays significantly impacts the performance of commercial boost converter circuits, with gamma radiation identified as the primary driver of transient behavior and circuit failure. Results from live monitoring at PUR-1 and the Co-60 irradiator highlight that degradation manifests as an increase in output voltage followed by abrupt circuit failure, typically associated with MOSFET burnout for high TID. Thermal neutron effects, particularly through induced activation, contribute to secondary gamma exposure, potentially compounding TID effects. Cadmium shielding experiments further revealed that attenuation of thermal neutrons leads to deviations in degradation trends, suggesting synergistic interactions in mixed radiation fields. The findings advocate for the use of accessible thermal neutron reactors for early-stage identification of radiation-sensitive electronics, potentially accelerating the development cycle for radiation-hardened systems. Future research should expand on shielding strategies and material activation impacts to better isolate and understand particle-specific damage mechanisms.

Acknowledgment

This work would not be possible without the Major David Fobar, United States Army, for his contribution to the SCRAM chip designed under DTRA/NSERC. Additionally, the Purdue Military Research Institute for providing their support towards this research. Furthermore, the United States Navy for Naval NISE/219 funding. Finally, True Miller and Brian Jowers III,

Reactor staff, for their MCNP model and operation of PUR-1.

REFERENCES

[1] A. H. Johnston, "Radiation effects in advanced microelectronics technologies," in *RADECS 97. Fourth European Conference on Radiation and its Effects on Components and Systems (Cat. No.97TH8294)*, Cannes, France: IEEE, 1998, pp. 1–16. doi: 10.1109/RADECS.1997.698828.
[2] A. Cester and A. Paccagnella, "IONIZING RADIATION EFFECTS ON ULTRA-THIN OXIDE MOS STRUCTURES," *Int. J. Hi. Spe. Ele. Syst.*, vol. 14, no. 02, pp. 563–574, June 2004, doi: 10.1142/S012915640400251X.
[3] S. C. Hanson, Y. Xiao, R. Charrette, and R. B. Hayes, "A preliminary NASA compliant conformal coating for optimized space radiation shielding configurations and its mass attenuation coefficients," *Progress in Nuclear Energy*, vol. 169, p. 105089, Apr. 2024, doi: 10.1016/j.pnucene.2024.105089.
[4] Y. Q. D. Aguiar, F. Wrobel, J.-L. Autran, and R. García Alía, *Single-Event Effects, from Space to Accelerator Environments: Analysis, Prediction and Hardening by Design*. Cham: Springer International Publishing, 2025. doi: 10.1007/978-3-031-71723-9.
[5] C. De Sio, S. Azimi, L. Sterpone, and B. Du, "Analyzing Radiation-Induced Transient Errors on SRAM-Based FPGAs by Propagation of Broadening Effect," *IEEE Access*, vol. 7, pp. 140182–140189, 2019, doi: 10.1109/ACCESS.2019.2915136.
[6] M. E. Şahin and F. Blaabjerg, "An Overview on MOSFET Drivers and Converter Applications," *Electric Power Components and Systems*, vol. 49, no. 8, pp. 828–847, May 2021, doi: 10.1080/15325008.2021.2002477.
[7] J. J. Liou and F. Schwierz, "RF MOSFET: recent advances, current status and future trends," *Solid-State Electronics*, vol. 47, no. 11, pp. 1881–1895, Nov. 2003, doi: 10.1016/s0038-1101(03)00225-9.
[8] S. M. A. El-Azeem and W. A. El-Basit, "Impact of gamma-ray irradiation on commercial silicon carbide MOSFET with boost converter application," *Power Electronic Devices and Components*, vol. 10, p. 100077, Mar. 2025, doi: 10.1016/j.pedc.2025.100077.
[9] B. Djezzar, A. Smatti, A. Amrouche, and M. Kechouane, "Channel-length impact on radiation-induced threshold-voltage shift in N-MOSFET devices at low gamma ray radiation doses," *IEEE Trans. Nucl. Sci.*, vol. 47, no. 6, pp. 1872–1878, Dec. 2000, doi: 10.1109/23.914462.
[10] Z. An *et al.*, "The impact of TID effect on EMS of PDSOI voltage reference circuits," in *2018 IEEE International Symposium on Electromagnetic Compatibility and 2018 IEEE Asia-Pacific Symposium on Electromagnetic Compatibility (EMC/APEMC)*, Singapore: IEEE, May 2018, pp. 852–856. doi: 10.1109/ISEMC.2018.8393902.
[11] P. C. Adell *et al.*, "Total-dose and single-event effects in switching DC/DC power converters," *IEEE Trans. Nucl. Sci.*, vol. 49, no. 6, pp. 3217–3221, Dec. 2002, doi: 10.1109/TNS.2002.805425.
[12] L. Lv *et al.*, "Fast and Thermal Neutron Radiation Effects on GaN PIN Diodes," *IEEE Trans. Nucl. Sci.*, vol. 64, no. 1, pp. 643–647, Jan. 2017, doi: 10.1109/TNS.2016.2630061.
[13] R. Miteva, S. W. Samwel, and S. Tkatchova, "Space Weather Effects on Satellites," *Astronomy*, vol. 2, no. 3, pp. 165–179, Aug. 2023, doi: 10.3390/astronomy2030012.
[14] E. E. Conrad, "Radiation effects research in the 60's," *IEEE Trans. Nucl. Sci.*, vol. 41, no. 6, pp. 2648–2659, Dec. 1994, doi: 10.1109/23.340627.
[15] J. R. Srour, "Radiation effects R&D in the 1970s: a retrospective view," *IEEE Trans. Nucl. Sci.*, vol. 41, no. 6, pp. 2660–2665, Dec. 1994, doi: 10.1109/23.340628.
[16] D. Binder, E. C. Smith, and A. B. Holman, "Satellite Anomalies from Galactic Cosmic Rays," *IEEE Trans. Nucl. Sci.*, vol. 22, no. 6, pp. 2675–2680, 1975, doi: 10.1109/tns.1975.4328188.
[17] D. J. Cochran *et al.*, "Recent Total Ionizing Dose and Displacement Damage Compendium of Candidate Electronics for NASA Space Systems," in *2011 IEEE Radiation Effects Data Workshop*, Las Vegas, NV: IEEE, July 2011, pp. 1–10. doi: 10.1109/REDW.2010.6062498.
[18] R. L. Pease, A. H. Johnston, and J. L. Azarewicz, "Radiation testing of semiconductor devices for space electronics," *Proc. IEEE*, vol. 76, no. 11, pp. 1510–1526, 1988, doi: 10.1109/5.90110.
[19] General Atomics, "TRIGA Nuclear Reactors." Accessed: July 09, 2025. [Online]. Available: https://www.ga.com/triga/
[20] U.S Government, "Framatome Makes First TRIGA Fuel for U.S. Research Reactors." Accessed: July 09, 2025. [Online]. Available: https://www.energy.gov/ne/articles/framatome-makes-first-triga-fuel-us-research-reactors
[21] T. Elbashbishy and I. H. El-adaway, "Skilled Worker Shortage across Key Labor-Intensive Construction Trades in Union versus Nonunion Environments," *J. Manage. Eng.*, vol. 40, no. 1, Jan. 2024, doi: 10.1061/jmenea.meeng-5649.
[22] Matt Kay, "Strategic Radiation Hardened (SRH) Electronics Council (SRHEC)," NASA Goddard Space Flight Center, June 06, 2019. [Online]. Available: https://nepp.nasa.gov/workshops/etw2019/talks.../0617MON/1130%20-%20Kay%20-%20SRHEC%20NEPP.pdf
[23] Kenneth A. LaBel, "External Radiation Test Facilities for Testing of Electronics: NASA Overview with Emphasis on Single Event Effects (SEE)," presented at the Study on Space Radiation Effects Test Infrastructure (Electronics) Meeting, Washington DC, Mar. 29, 2017. [Online]. Available: https://nepp.nasa.gov/files/28793/NEPP-CP-2017-LaBel-NSA-Pres-TN40074.pdf
[24] D. M. Fleetwood and H. A. Eisen, "Total-dose radiation hardness assurance," *IEEE Trans. Nucl. Sci.*, vol. 50,

no. 3, pp. 552–564, June 2003, doi: 10.1109/TNS.2003.813130.

[25] M. Niichel, “Development Of An Electronics Testbed For Radiation Testing In Gamma And Neutron Environments,” Purdue University, West Lafayette, IN, 2024.

[26] N. Pushpa and A. P. Gnana Prakash, “The influence of radiation on the electrical characteristics of MOSFET and its revival by different annealing techniques,” *Radiation Effects and Defects in Solids*, vol. 177, no. 3–4, pp. 392–400, Apr. 2022, doi: 10.1080/10420150.2022.2039930.

[27] M. M. Pejović, “Processes in radiation sensitive MOSFETs during irradiation and post irradiation annealing responsible for threshold voltage shift,” *Radiation Physics and Chemistry*, vol. 130, pp. 221–228, Jan. 2017, doi: 10.1016/j.radphyschem.2016.08.027.

[28] “Test Methods For Semiconductor Devices.” Department of Defense, Feb. 23, 1983. [Online]. Available: https://www.navsea.navy.mil/Portals/103/Documents/NSWC_Crane/SD-18/Test%20Methods/MILSTD750.pdf

[29] M. Niichel *et al.*, “Design and Characterization of the Modified Purdue Subcritical Pile for Nuclear Research Applications,” *Instruments*, vol. 9, no. 2, p. 13, June 2025, doi: 10.3390/instruments9020013.

[30] “Standard Test Method for Determining Thermal Neutron Reaction Rates and Thermal Neutron Fluence Rates by Radioactivation Techniques.” Accessed: Aug. 29, 2024. [Online]. Available: https://www.astm.org/e0262-17.html

[31] “Standard Practice for Characterizing Neutron Fluence Spectra in Terms of an Equivalent Monoenergetic Neutron Fluence for Radiation- Hardness Testing of Electronics1,” American Society for Testing and Materials, E722-09, Dec. 2010.

[32] J. A. Kulesza *et al.*, *MCNP® Code Version 6.3.0 Theory & User Manual*. (Sept. 2022). Los Alamos National Laboratory Tech. Rep., Los Alamos, NM, USA.

[33] Maxim Integrated Products, “MAX1932 Digitally Controlled, 0.5% Accurate, Safest APD Bias Supply.” 2019. [Online]. Available: https://www.analog.com/media/en/technical-documentation/data-sheets/max1932.pdf

[34] Infineon Technologies AG, “OptiMOS™ Small-Signal-Transistor.” 2012. [Online]. Available: https://www.mouser.com/datasheet/2/196/Infineon-BSS119N-DS-v02_01-en-773952.pdf

[35] V. Danchenko, U. D. Desai, and S. S. Brashears, “Characteristics of Thermal Annealing of Radiation Damage in MOSFET’s,” *Journal of Applied Physics*, vol. 39, no. 5, pp. 2417–2424, Apr. 1968, doi: 10.1063/1.1656570.

[36] J. W. Mietelski, “Detection of background thermal neutrons in a modified low-background germanium gamma-ray spectrometer,” *J Radioanal Nucl Chem*, vol. 322, no. 3, pp. 1331–1339, Dec. 2019, doi: 10.1007/s10967-019-06843-9.

[37] J.-Ch.Sublet, J.A. Simpson, R.A.Forrest, and D. Nierop, “NGAtlas.” International Atomic Energy Agency, Sept. 2001. [Online]. Available: https://www-nds.iaea.org/ngatlas2/atlas.htm

[38] V. F. Sears, “Neutron scattering lengths and cross sections,” *Neutron News*, vol. 3, no. 3, pp. 26–37, Jan. 1992, doi: 10.1080/10448639208218770.

[39] “An Introduction to X-Ray Fluorescence (XRF) Analysis in Archaeology,” in *X-Ray Fluorescence Spectrometry (XRF) in Geoarchaeology*, New York, NY: Springer New York, 2011, pp. 7–44. doi: 10.1007/978-1-4419-6886-9_2.